

RSC Advances



This is an *Accepted Manuscript*, which has been through the Royal Society of Chemistry peer review process and has been accepted for publication.

Accepted Manuscripts are published online shortly after acceptance, before technical editing, formatting and proof reading. Using this free service, authors can make their results available to the community, in citable form, before we publish the edited article. This *Accepted Manuscript* will be replaced by the edited, formatted and paginated article as soon as this is available.

You can find more information about *Accepted Manuscripts* in the [Information for Authors](#).

Please note that technical editing may introduce minor changes to the text and/or graphics, which may alter content. The journal's standard [Terms & Conditions](#) and the [Ethical guidelines](#) still apply. In no event shall the Royal Society of Chemistry be held responsible for any errors or omissions in this *Accepted Manuscript* or any consequences arising from the use of any information it contains.



Nitrogen-doped carbon decorated $\text{Li}_4\text{Ti}_5\text{O}_{12}$ composites as anode materials for high performance lithium-ion batteries

Feng Wang^a, Liangcheng Luo^a, Jun Du^a, Liangui Guo^a, Bihui Li^a, Yu Ding^{a,b*}

Received 00th January 2015,
Accepted 00th January 2015

DOI: 10.1039/x0xx00000x

www.rsc.org/

Nitrogen-doped carbon nanomaterials (NC), originating from melamine, decorated nano- $\text{Li}_4\text{Ti}_5\text{O}_{12}$ composites (LTO/NC) have been prepared by a simple high-energy ball milling with further heat treatment under nitrogen atmosphere. The as-prepared LTO/NC composites had a regular structure with a size of 300 to 500 nm. The optimum designed LTO/NC composites showed the best performance with a high rate capacity of 161.5 mAh g^{-1} at 1 C and showed excellent stability with 97.2% capacity retention after 100 cycles, as well as a remarkable rate capacity by maintaining 103 mAh g^{-1} of the capacity at 20 C. The composites also exhibited excellent performances because of the NC decoration, which enhanced the electrochemical reactivity and electronic conductivity. These results provide a facile, general, and cost-effective strategy for the synthesis of LTO composites anode materials for high-performance lithium-ion batteries.

Introduction

With the increasing applications of electric vehicles and portable electric devices, lithium-ion batteries (LIBs) with high energy and power density are extremely considered as the most suitable candidates.¹⁻³ Among the various electrode materials, $\text{Li}_4\text{Ti}_5\text{O}_{12}$ (LTO) has been extraordinarily investigated for LIBs because of its excellent reversibility, relatively higher operating voltage (1.55 V vs. Li/Li^+), and high safety and thermodynamic stability.⁴⁻⁷ More importantly, the solid-electrolytes interphase (SEI) layer does not form during the lithiation and delithiation processes.⁸ However, the poor intrinsic electrical conductivity ($<10^{-13} \text{ S cm}^{-1}$) and the moderate Li^+ diffusion coefficient (10^{-9} to $10^{-13} \text{ cm}^2 \text{ s}^{-1}$) of LTO seriously hinder its scalable application as high energy density and rate performance batteries.

Various effective strategies have been performed to improve the rate capability and shorten the distance of the Li^+ and electron transport, such as nanostructure reconstruction, doping, and coating.⁹⁻¹³ Carbon-coated LTO nanostructures have been demonstrated to improve electrochemical performance.¹⁴⁻¹⁶ In fact, coated carbon layer, which originates from organic compounds, cannot be completely graphitized under the common synthesis temperature ($<1000 \text{ }^\circ\text{C}$), which causes the low conductivity of the carbon layer. At present, hetero-atoms (such as N and B) doped

carbon materials are widely used to enhance electrochemical reactivity and electronic conductivity.^{17,18} NC materials can induce significant defects and form a disordered carbon structure to stabilize the anode structure, which may serve as additional active sites for enhancing lithium storage properties and preventing the collapse of the anode structure. Moreover, NC can increase the interlayer distance, ensuring the penetration of Li^+ .¹⁹ Thus, adopting advanced hetero atoms doped carbonaceous materials to coat the nanostructure LTO anode for enhancing electrochemical performances is worthwhile. In the present work, we design a facile way to prepare the NC-coated LTO nanomaterials using melamine as the nitrogen and carbon sources. Melamine is one of the superior N contents (about 67%) and low cost organic compounds. Electrochemical studies show the promising capacity and stability of the NC-decorated LTO nanomaterials for LIBs.

Experimental section

Preparation of pristine $\text{Li}_4\text{Ti}_5\text{O}_{12}$ (LTO) and nitrogen-doped carbon nanomaterials decorated $\text{Li}_4\text{Ti}_5\text{O}_{12}$ (LTO/NC)

The pristine LTO was prepared through a typical wet-milling procedure as the follows: 5 mmol TiO_2 nanospheres with the diameter 100–200 nm diameters were mixed with a 4.05 mmol LiOH in 20 mL ethanol and redistilled water (1:1, in volume) mixed solution, which was milled by high energy mechanical-milling (the ball-to-power weight ratio of 20:1). The after-milling mixture was dried at $60 \text{ }^\circ\text{C}$ overnight, sintered at $700 \text{ }^\circ\text{C}$ for 3 h in air, and naturally cooled.

To prepare the LTO/NC cathode composites, LiOH , TiO_2 nanospheres, (molar ratio of $\text{Li}:\text{Ti} = 4.05:5$) and melamine were used as the starting material. Melamine was used as the nitrogen and carbon source. The weight ratios of melamine and the two salts were 2.5%, 5%, 7.5% and 10%, respectively. The reactors were

^a College of Chemistry and Materials Science, Hubei Engineering University, Xiaogan 432000, China.

^b State Key Laboratory of Materials Processing and Die & Mould Technology, School of Materials Science and Engineering, Huazhong University of Science and Technology, Hubei 430074, China.

* Corresponding author. E-mail addresses: dy9802@126.com (Y. Ding); Tel: +86 712 2345464; fax: +86 712 2345265.

† Electronic Supplementary Information (ESI) available: XPS of the LTO and the Coulombic efficiency of LTO-2. See DOI: 10.1039/x0xx00000x

mixed by high energy mechanical-milling (the ball-to-power weight ratio of 20:1) in 20 mL ethanol and redistilled water (1:1, in volume) to ensure homogeneous mixing. The mixture was dried at 60 °C overnight, sintered at 700 °C for 3 h in N₂, and naturally cooled. The final composites were named LTO-1, LTO-2, LTO-3, and LTO-4, respectively.

Physical characterization

The materials were characterized by X-ray diffraction measurement (XRD, Bruker D8 Advance using Cu K α radiation, within the 10.00°–80.00° 2 θ range), scanning electron microscopy (SEM, Hitachi S3400N), high-resolution transmission electron microscopy (HR-TEM, JEOL JEM-2010), inductively coupled plasma emission spectroscopy (ICP, OPTIMA 8000DV), thermogravimetric analyses (TG, SDT Q600, 10 °C·min⁻¹ from room temperature to 800 °C under air or nitrogen atmosphere with an air or nitrogen flow rate of 20 mL·min⁻¹), and Raman measurements (Raman, LabRAM HR Evolution, equipped with a laser that provide excitation wavelength at 633 nm). X-ray photoelectron spectroscopy (XPS) measurements were carried out by a Kratos Axis UltraDLD spectrometer (Kratos Analytical-A Shimadzu group company) using a monochromatic Al K α radiation ($h\nu = 1486.6$ eV). The binding energies of the samples were calibrated by taking C1s peak as a reference (284.6 eV).

Electrochemical tests

Electrochemical performances of the composites were performed with a CR2016-type coin cell battery. The electrode was fabricated by pasting a mixture of 85% active material, 10% super P, and 5% polyvinylidene fluoride on a copper foil and dried at 100 °C for 5 h in vacuum. The thickness and radius of the electrodes are about 100 μ m and 1 cm, respectively. Metallic lithium slice was used as the counter electrode. The electrolyte was 1 mol L⁻¹ LiPF₆ in mixed solvents of ethylene carbonate (EC)/dimethyl carbonate (DMC)/ethylmethyl carbonate (EMC) (1:1:1, in volume); and Celgard 2400 membrane was used as the separator. The cells were assembled in an argon-filled glove box (Mikrouna Universal 2440/750). The galvanostatic charge and discharge experiments were performed at a rate of 1–20 C between cutoff voltages of 1.0 V and 2.5 V on a LAND-CT2001A battery-testing system. Cyclic voltammetry (CV) was performed at different scan rates with a CHI660E electrochemical workstation (CHI Instruments TN). Electrochemical impedance spectroscopy (EIS) was performed to compare the conductivities at an amplitude of 5 mV and frequencies ranging from 100 kHz to 100 mHz.

Results and discussion

Our strategy for preparing the LTO/NC composites consists of two steps. First, the precursors are mixed through wet-ball milling with water/ethanol. Second, the mixture is sintered at 700 °C in air (LTO) or nitrogen (LTO/NC) atmosphere. In these processes, melamine is used as the nitrogen and carbon sources. Notably, there are not needed templates substances and rigorous conditions, which provide a facile and cost-effective strategy for the

synthesis of LTO composites anode material for high-performance LIBs.

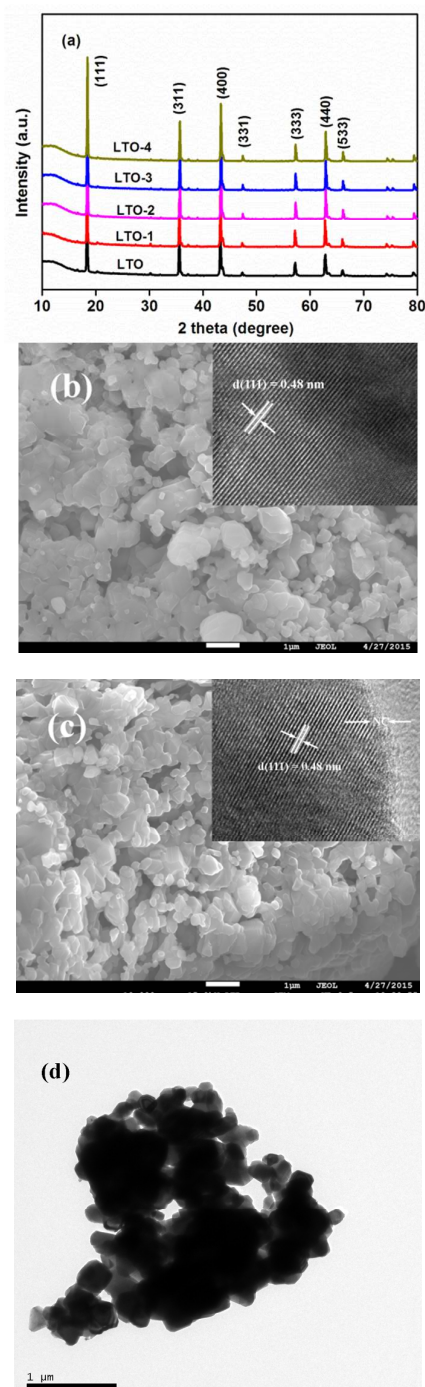


Fig. 1 The X-ray diffraction of the pristine LTO and LTO/NC (a), SEM images and HR-TEM images of pristine LTO (b) and LTO-2 (c), TEM image of LTO-2 (d).

The XRD, SEM, and TEM patterns of the as prepared LTO and LTO/NC are shown in Fig. 1. The XRD diffraction peaks (Fig. 1a) of the synthesized LTO and LTO/NC composites at $2\theta = 18.4, 35.6, 43.2, 47.3, 57.2, 62.8,$ and 66.1 belonged to the (111), (311), (400), (331), (333), (440), and (533) planes, which can be indexed as the

face-centered cubic spinel phase LTO (*Fd3m* space group, JCPDS No. 49-0207). Secondary phase peaks, such as TiO_2 or Li_2TiO , were not detected, indicating the purity of the LTO phase. However, no

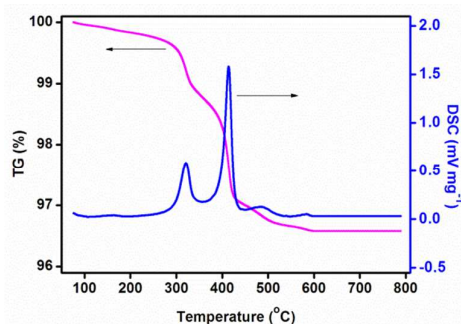


Fig. 2 The TG-DSC curves of LTO-2.

obvious peaks correspond to NC because of its low content. The obvious difference is that the white LTO becomes black after NC coating. Moreover, the lattice parameter a had a slight change of LTO (0.8349 nm) and LTO-2 (0.8337 nm), obtained by analyzing the XRD pattern, which indicates that the LTO/NC nanoparticles were small. The ICP results indicate that the mole ratio of Li: Ti was 0.78, which is close to that in $\text{Li}_4\text{Ti}_5\text{O}_{12}$. Well-defined crystals are shown in Fig. 1c. The nanoparticles reveal quite uniform sizes, at 300–500 nm. After being decorated by NC, the SEM image exhibited more uniform of LTO. Furthermore, the TEM image (Fig. 1d) shows that the LTO nanoparticles dispersed in the NC matrix. The HR-TEM image (Fig. 1c, inset) clarify that the LTO-2 is surrounded by a thin layer NC with the thickness of about 2 nm. The lattice spacing of 0.48 nm corresponds to the (111) plane of LTO (Fig. 1b, inset), which is not changed in LTO-2.

The dehydration processes of LTO-2 were investigated by TG-DSC analysis. The TG curve of the LTO-2 shown in Fig 2 indicates that a sharp weight loss near 200 °C continued until 500 °C, which can be attributed to the skeleton degradation and the slow oxidation and decomposition of the NC material.²⁰ The strong endothermic peak at between about 200 and 500 °C corresponds with the decomposition of the melamine from NC. After 600 °C, there was no weight loss in further temperature increases. The TG-DSC analysis indicates that the amount of NC in LTO-2 was estimated to be 3.11 wt%, which is in according with the element analysis of 3.53%.

The XPS survey spectra of LTO-2 are shown in Fig. 3. The wide survey spectrum confirmed the presence of Ti, O, N, and C elements in LTO-2. The high resolution Ti2p spectrum (Fig. 3b) exhibits two peaks at 464.1 eV (Ti2p1/2) and 458.3 eV (Ti2p3/2), which is in accordance with the previous reports.^{5,21} The Ti2p3/2 peak of Ti^{3+} is located at about 458.0 eV.²¹ Accordingly, the Ti2p3/2 peak of the LTO and LTO-2 at 458.0 eV and 458.3 eV represents a state close to Ti^{3+} (ESI Fig. S1), respectively. After the NC decorated, the partial reduction of Ti^{4+} on the LTO surface to Ti^{3+} would enhance the electronic conductivity.²¹ The high resolution C1s spectrum (Fig. 3c) can be deconvoluted into four peaks. The two stronger peaks at 284.2 and 285.1 eV may be attributed to the sp^2 -hybridized graphite carbon

and the sp^3 -hybridized diamond carbon, respectively, whereas the weaker ones may have originated from the oxygenated carbon atoms (285.6 eV for C–O; 288.3 eV for C=O).^{22,23} The peak of N1s

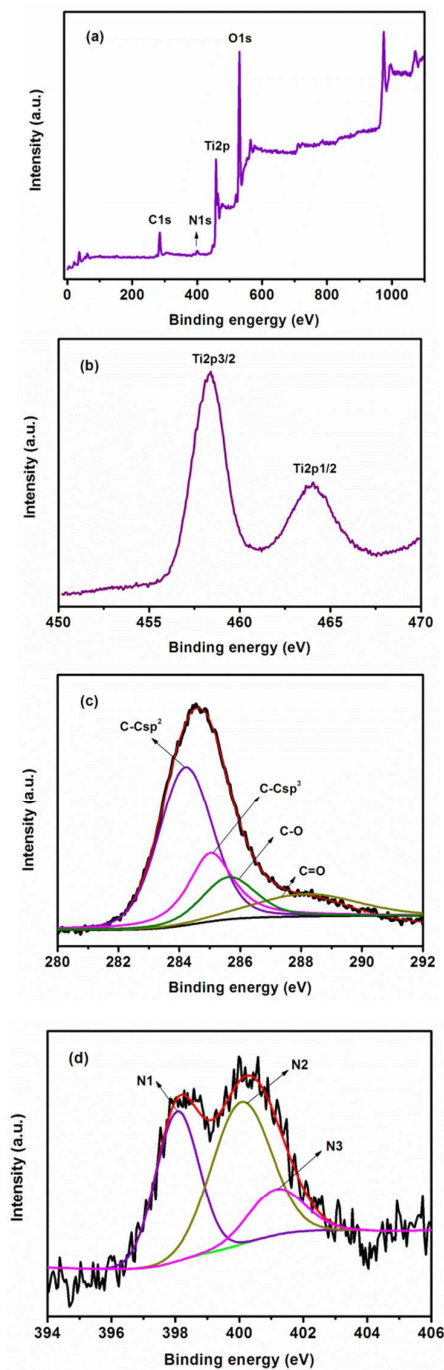


Fig. 3 The X-ray photoelectron spectroscopy of LTO-2.

that appeared in the XPS indicates that the LTO surface was doped with nitrogen. In the high resolution N1s spectrum (Fig. 3d), two peaks at 398.1 and 400.1 eV may belong to pyridinic nitrogen (N1) and pyrrolic nitrogen (N2), respectively, and the peak at the binding energy of 401.3 eV may indicate the presence of quaternary

nitrogen (N3).^{20,24} The three different types of nitrogen doping in the carbon layer cause the defects in the symmetrical arrangement of aromatic rings carbon.²⁵ These defects can enhance the penetration of Li^+ in the LTO bulk.^{19,20}

bands. The Raman spectra of LTO-2 display the G band at 1598 cm^{-1} and D band at 1395 cm^{-1} , and the peak intensity ratio (I_D/I_G) is 0.71, which indicates that a considerable amount of structure defects exists in the LTO/NC composites.²⁶⁻²⁸

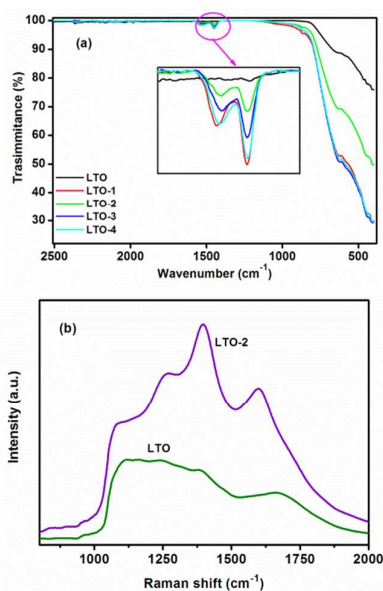


Fig.4 The Fourier transform infrared spectroscopy (a) and Raman spectra (b) of the bare LTO and LTO/NC composites.

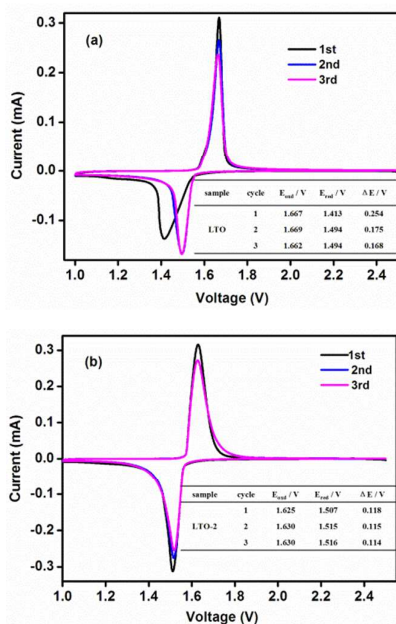


Fig.5 Cyclic voltammograms curves of LTO (a) and LTO-2 (b).

The FT-IR and Raman spectra of the LTO and LTO/NC composites are shown in Fig. 4. Compared with that of the bare LTO, the characteristic features of the composites with C=N or C=O stretching vibration ($1500\text{--}1715\text{ cm}^{-1}$) are present.²² There are strong peaks at 927 and 623 cm^{-1} in the precursor and final composites, which are attributed to the Li–O and Ti–O stretching

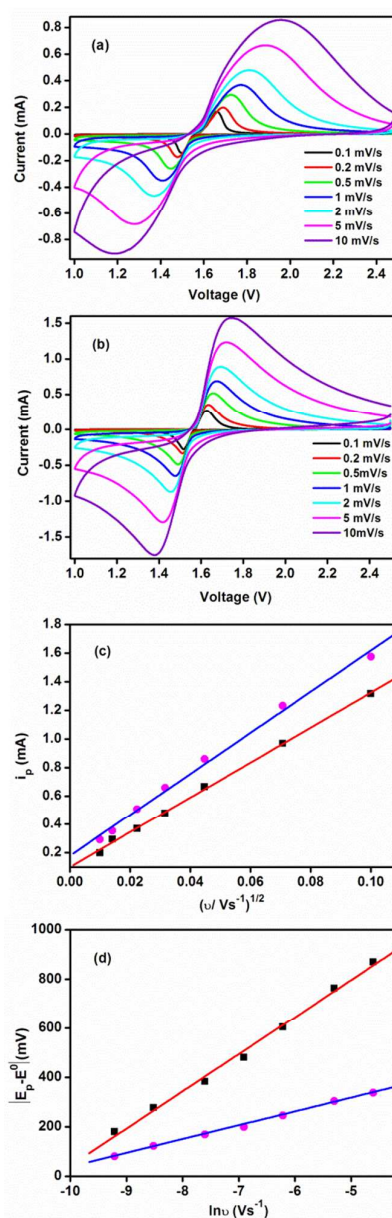


Fig.6 Cyclic voltammetry curves of the bare LTO (a) and LTO-2 (b) at an increasing scan rate from 0.5 to 2 mV s^{-1} , respectively; A linear relationship between i_p and scan rate $v^{1/2}$ is detected for the bare LTO and LTO-2 (c); The plots of $|E_p - E^0|$ vs. $\ln v$ for the bare LTO and LTO-2 (d).

The electrochemical performances of LTO and LTO/NC were systematically investigated using a coin-type half cell. The cyclic voltammograms (CVs) curves of LTO and LTO-2 are shown in Fig. 5. There was a pair of similar reversible redox peaks at 1.70 V (vs. Li/Li^+) and 1.45 V (vs. Li/Li^+) for LTO and LTO-2, which correspond to the processes of Li deintercalation and intercalation,⁹ respectively, as shown in reaction (1).²⁹ The cathodic and anodic peaks of the

LTO-2 are much stronger and sharper than that of the LTO, which indicate the better electrode kinetic of the LTO/NC. In addition, the potential differences between the cathodic and anodic peaks of LTO and LTO-2 are 0.25 and 0.15 V, respectively, which suggests that N-doping could improve the electronic conductivity, easy kinetic

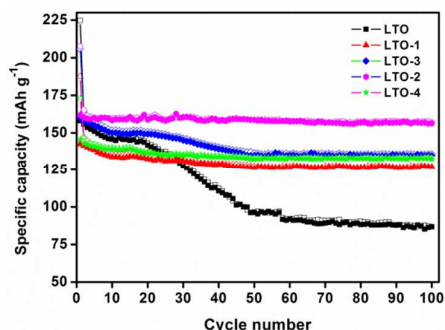


Fig. 7 Cycling performance of LTO and LTO/NC at 1 C rate.

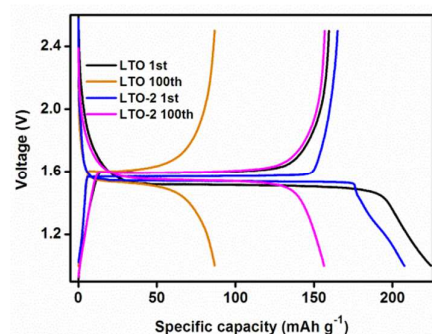


Fig. 8 The initial and after 100 charge/discharge cycles electrochemical performances profiles of the LTO and LTO-2 at 1 C rate.

properties, and good stability of materials and is favorable for reducing the electrode polarization.^{30,31}

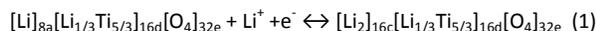


Fig. 6 shows the cyclic voltammetry curves of LTO and LTO-2 at an increasing scan rate of 0.1 to 10 $\text{mV}\cdot\text{s}^{-1}$. A linear relationship between the i_p and scan rate $u^{1/2}$ was detected for LTO and LTO-2, as shown in Fig. 6c. The diffusion constant for the Li^+ ions in the LTO-2 was calculated according to the Randles-Sevcik equation,^{32,33} $i_p = 268600 n^{3/2} A D^{1/2} C_{\text{Li}} u^{1/2}$. The lithium diffusion coefficients of lithium (D_{Li}) of LTO and LTO-2 were 1.15×10^{-15} and 1.62×10^{-14} $\text{cm}^2\cdot\text{s}^{-1}$, respectively. Therefore, the NC that originated from the melamine in LTO-2 was uniform, and with a larger lithium ion diffusion coefficient and higher electronic conductivity than that of the LTO.²¹ Fig. 6d shows the plots of $|E_p - E^0|$ versus $\ln u$ for the pristine LTO and LTO-2. Both plots showed good linearity within the entire range of scan rates studied, which means that the electrochemical reaction of LTO and LTO/NC is a single electron pseudo first-order reaction and the lithiation and delithiation processes are pseudo reversible.

The LTO and LTO/NC composites were further subjected to cycling performance evolutions at 1 C for 100 cycles, as shown in Fig. 7. At 1 C, LTO/NC composites exhibited better electrochemical

performances than the pristine LTO. The LTO-2 showed the best electrochemical performances and reached a reversible capacity of $156.9 \text{ mAh}\cdot\text{g}^{-1}$ after 100 cycles, which retained 97.2% of its initial discharge capacity ($161.5 \text{ mAh}\cdot\text{g}^{-1}$) and the Coulombic efficiency was almost 100% (ESI Fig. S2). While reconsidering the cycling performance of the pristine LTO, the initial discharge capacity was

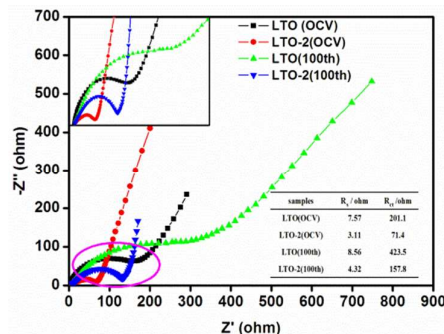


Fig. 9 The electrochemical impedance spectroscopy of LTO and LTO-2 at OCV and after 100 charge/discharge cycles.

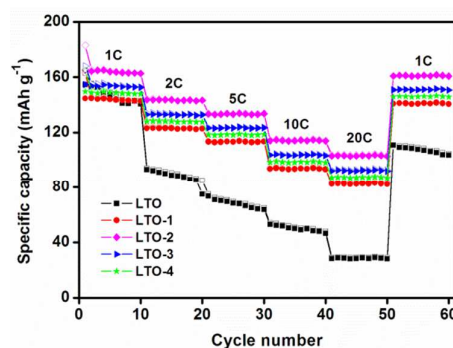


Fig. 10 The rate capabilities of the pristine LTO and LTO/NC electrodes

224.8 and $86.8 \text{ mAh}\cdot\text{g}^{-1}$ after 100 cycles, which is only one third of the initial cycle. Fig. 8 shows the initial and after 100 charge/discharge cycles electrochemical performances profiles of the LTO and LTO-2 at 1 C rate. Both electrodes presented voltage plateaus around 1.55 V, which agrees with the CVs results. Obviously, LTO-2 presents a flatter plateau profile and a larger plateau capacity than the bare LTO, and the potential differences between the charge and discharge plateau was 80 mV (1.59–1.51) for LTO and only 20 mV (1.56–1.54) for LTO-2, which became 110 mV (1.62–1.51) of LTO and 60 mV (1.60–1.54) of LTO-2 even after 100 charge/discharge cycles, as shown in Fig. 8. The potential plateau of the pristine LTO became shorter and slightly bent down, while that of the LTO-2 remained flat.

The EIS of LTO and LTO-2 at the open circuit voltage (OCV) and after 100 charge/discharge cycles are shown in Fig. 9. Both EIS profiles were composed of a depressed semicircle at high frequencies and a spike at low frequencies. LTO-2 evidently had a smaller charge-transfer resistance (R_{ct} , 71.4 and 157.8 ohm) and seclusion resistance (R_s , 3.11 and 4.32 ohm) than those of the pristine one (201.1 and 423.5 ohm, and 7.57 and 8.56 ohm,

respectively), which was ascribed to the enhanced electronic contacts between the LTO particles because of the presence of highly conductive NC.³⁴ The decrease in R_{ct} was probably expected to overcome the kinetics restrictions in the process of charge/discharge and consequently enlarge the depth of Li-ion insertion/extraction.

Fig. 10 compares the rate capabilities of pure LTO and LTO/NC electrodes. For each stage, the charge-discharge processes of the samples were taken at 10 cycles. The LTO/NC composites exhibited excellent electrochemical performances. The LTO-2 electrode delivered capacities of 165.2, 143.7, 133.4, 114.3, and 103.1 mAh g^{-1} at 1, 2, 5, 10 C, and 20 C, respectively. As for the bare LTO electrode, the capacities were 154.7, 93.2, 73.4, 53.1, and 28.3 mAh g^{-1} , respectively. Moreover, as the current rate returned to 1 C, a stable capacity of 161.6 mAh g^{-1} was obtained with rare decaying in the following 10 cycles, demonstrating that the LTO/NC electrode has an excellent reversibility and stability.

The high specific capacity, extraordinary cyclability, and superior rate capability of LTO/NC composites make them potential anode materials for commercial LIBs. Accompanying the simple annealed process, the NC layers were dispersed uniformly on the surface of LTO, which favoured the quick migration of the inserted Li ion, increasing the Li ion diffusion coefficient and electronic conductivity, and reducing the polarization. Therefore, the synergetic effects of NC and LTO can enhance the high capacity and impressive rate capability.

Conclusions

NC material decorated $\text{Li}_4\text{Ti}_5\text{O}_{12}$ nanograins were successfully prepared via a simple high-energy ball milling, followed by sintering in N_2 atmosphere. NC is beneficial in improving the conductivity of the composite. When LTO/NC composites were used as anode for LIBs, LTO-2 showed a better rate capability and cycle stability. After 100 cycles, its discharge capacity was 156.9 mAh g^{-1} at 1 C. The specific capacity of LTO-2 was 103 mAh g^{-1} even at the rate of 20 C. The excellent rate capability can be attributed to the enhanced conductivity of the N-doped modification combined with the short ion and electron transfer paths of nanomaterials. Therefore, we provide a facile and cost-effective strategy for the synthesis of LTO composites anode material for high performance LIBs.

Acknowledgements

The authors are thankful for the financial support from the National Nature Science Foundation of China (21301054 and 51402096), the Nature Science Foundation of Hubei Province of China (2012FFB00503) and the Science and Technology Foundation of the department of education of Hubei Province (Q20132702).

References

- 1 Y. Y. Hu, Z. G. Liu, K. W. Nam, O. J. Borkiewicz, J. Cheng, X. Hua, M. T. Dunstan, X. Q. Yu, K. M. Wiaderek, L. S. Du, K. W.

- Chapman, P. J. Chupas, X. Q. Yang and C. P. Grey, *Nat. Mater.*, 2013, **12**, 1130-1136.
- 2 Z. Liu, J. Xu, D. Chen and G. Z. Shen, *Chem. Soc. Rev.*, 2015, **44**, 161-192.
- 3 J. A. Rogers, T. Someya and Y. G. Huang, *Science*, 2010, **327**, 1603-1607.
- 4 Q. Zhou, L. Liu, H. P. Guo, R. Xu, J. L. Tan, Z. C. Yan, Z. F. Huang, H. B. Shu, X. K. Yang and X. Y. Wang, *Electrochim. Acta*, 2015, **151**, 502-509.
- 5 X. L. Jia, Y. F. Kan, X. Zhu, G. Q. Ning, Y. F. Lu and F. Wei, *Nano Energy*, 2014, **10**, 344-352.
- 6 W. N. Chen, H. Jiang, Y. J. Hu, Y. H. Dai and C. Z. Li, *Chem. Commun.*, 2014, **50**, 8856-8859.
- 7 X. L. Jia, Y. F. Kan, X. Zhu, G. Q. Ning, Y. F. Lu and F. Wei, *Nano Energy*, 2014, **10**, 344-352.
- 8 J. B. Goodenough and Y. Kim, *J. Power Sources*, 2011, **196**, 6688-6694.
- 9 J. Liu, K. P. Song, P. A. van Aken, J. Maier and Y. Yu, *Nano Lett.*, 2014, **14**, 2597-2603.
- 10 F. L. Zhang, B. Xu, G. P. Cao, M. Chu, N. Qiao, G. Wei and Y. S. Yang, *Rsc Adv.*, 2014, **4**, 53981-53986.
- 11 X. N. Han, Z. Zhao, Y. L. Xu, D. Liu, H. Zhang and C. J. Zhao, *Rsc Adv.*, 2014, **4**, 41968-41975.
- 12 W. Wang, Y. Y. Guo, L. X. Liu, S. X. Wang, X. J. Yang and H. Guo, *J. Power Sources*, 2014, **245**, 624-629.
- 13 M. Krajewski, M. Michalska, B. Hamankiewicz, D. Ziolkowska, K. P. Korona, J. B. Jasinski, M. Kaminska, L. Lipinska and A. Czerwinski, *J. Power Sources*, 2014, **245**, 764-771.
- 14 Y. Wang, H. B. Rong, B. Z. Li, L. D. Xing, X. P. Li and W. S. Li, *J. Power Sources*, 2014, **246**, 213-218.
- 15 M. Lu, Y. Y. Tian, X. D. Zheng, J. Gao and B. Huang, *J. Power Sources*, 2012, **219**, 188-192.
- 16 B. H. Li, C. P. Han, Y. B. He, C. Yang, H. D. Du, Q. H. Yang and F. Y. Kang, *Energy Environ. Sci.*, 2012, **5**, 9595-9602.
- 17 C. Wang, Z. Y. Guo, W. Shen, Q. J. Xu, H. M. Liu and Y. G. Wang, *Adv. Funct. Mater.*, 2014, **24**, 5511-5521.
- 18 J. P. Paraknowitsch and A. Thomas, *Energy Environ. Sci.*, 2013, **6**, 2839-2855.
- 19 Z. Li, Z. W. Xu, X. H. Tan, H. L. Wang, C. M. B. Holt, T. Stephenson, B. C. Olsen and D. Mitlin, *Energy Environ. Sci.*, 2013, **6**, 871-878.
- 20 C. P. Han, Y. B. He, B. H. Li, H. F. Li, J. Ma, H. D. Du, X. Y. Qin, Q. H. Yang and F. Y. Kang, *ChemSuschem*, 2014, **7**, 2567-2574.
- 21 B. F. Wang, J. S. Wang, J. Cao, H. H. Ge and Y. F. Tang, *J. Power Sources*, 2014, **266**, 150-154.
- 22 H. S. Li, L. F. Shen, K. B. Yin, J. Ji, J. Wang, X. Y. Wang and X. G. Zhang, *J. Mater. Chem. A*, 2013, **1**, 7270-7276.
- 23 H. H. Xu, X. L. Hu, Y. M. Sun, W. Luo, C. J. Chen, Y. Liu and Y. H. Huang, *Nano Energy*, 2014, **10**, 163-171.
- 24 H. S. Li, L. F. Shen, J. Wang, B. Ding, P. Nie, G. Y. Xu, X. Y. Wang and X. G. Zhang, *ChemPluschem*, 2014, **79**, 128-133.
- 25 Z. H. Wang, L. Qie, L. X. Yuan, W. X. Zhang, X. L. Hu and Y. H. Huang, *Carbon*, 2013, **55**, 328-334.
- 26 F. Wang, W. Li, M. Y. Hou, C. Li, Y. G. Wang and Y. Y. Xia, *J. Mater. Chem. A*, 2015, **3**, 1703-1708.
- 27 W. Luo, X. L. Hu, Y. M. Sun and Y. H. Huang, *ACS Appl. Mat. Interfaces*, 2013, **5**, 1997-2003.
- 28 L. W. Su, Y. R. Zhong, J. P. Wei and Z. Zhou, *Rsc Adv.*, 2013, **3**, 9035-9041.
- 29 E. M. Sorensen, S. J. Barry, H. K. Jung, J. R. Rondinelli, J. T. Vaughey and K. R. Poeppelmeier, *Chem. Mater.*, 2006, **18**, 482-489.
- 30 J. W. Zhang, Z. Peng, W. Cai, L. G. Yu, Z. S. Wu and Z. J. Zhang, *Electrochim. Acta*, 2014, **132**, 230-238.
- 31 H. Q. Zhang, Q. J. Deng, C. X. Mou, Z. L. Huang, Y. Wang, A. J. Zhou and J. Z. Li, *J. Power Sources*, 2013, **239**, 538-545.

Journal Name

COMMUNICATION

- 32 Y. Shi, J. Gao, H. D. Abruna, H. Liu, H. J. Li, J. Z. Wang and Y. P. Wu, *Nano Energy*, 2014, **8**, 297-304.
- 33 W. J. Liu, D. Shao, G. E. Luo, Q. Z. Gao, G. J. Yan, J. R. He, D. Y. Chen, X. Y. Yu and Y. P. Fang, *Electrochim. Acta*, 2014, **133**, 578-582.
- 34 H. S. Li, L. F. Shen, X. G. Zhang, J. Wang, P. Nie, Q. Che and B. Ding, *J. Power Sources*, 2013, **221**, 122-127.